ACS APPLIED MATERIALS & INTERFACES

Research Article

www.acsami.org

# Carbon- and Oxygen-Free $Cu(InGa)(SSe)_2$ Solar Cell with a 4.63% Conversion Efficiency by Electrostatic Spray Deposition

Hyun Yoon,[†,◆] Seung Heon Na,[†,◆] Jae Young Choi,[†] Min Woo Kim,[†,‡] Hayong Kim,[†] Hee Sang An,[‡,§] Byoung Koun Min,[‡,§] SeJin Ahn,[∥] Jae Ho Yun,[∥] Jihye Gwak,[∥] KyungHoon Yoon,[∥] Sanjay S. Kolekar,[⊥] Maikel F. A. M. van Hest,[#] Salem S. Al-Deyab,[▽] Mark T. Swihart,[○] and Sam S. Yoon*[,†]

[†]School of Mechanical Engineering, Korea University, Anam-Dong, Seongbuk-Gu, Seoul 136-713, Korea

[‡]Green School, Korea University, Seoul 136-713, Republic of Korea

[§]Clean Energy Research Center, Korea Institute of Science & Technology, 39-1 Hawolgok-dong, Seongbuk-Gu, Seoul 136-791, Korea

[∥]Photovoltaic Research Center, Korea Institute of Energy Research, Yuseong-Gu, Dae-Jeon 305-343, Korea

[⊥]Department of Chemistry, Shivaji University, Kolhapur 416004, Maharashtra, India

[#]National Renewable Energy Laboratory, Golden, Colorado 80401, United States

[▽]Petrochem Research Chair, Department of Chemistry, College of Science, King Saud University, Riyadh 11451, Saudi Arabia

[○]Department of Chemical & Biological Engineering, University at Buffalo (SUNY), Buffalo, New York 14260, United States

**ABSTRACT:** We have demonstrated the first example of carbon- and oxygen-free $Cu(In,Ga)(SSe)_2$ (CIGSSe) absorber layers prepared by electrospraying a CuInGa (CIG) precursor followed by annealing, sulfurization, and selenization at elevated temperature. X-ray diffraction and scanning electron microscopy showed that the amorphous as-deposited (CIG) precursor film was converted into polycrystalline CIGSSe with a flat-grained morphology after post-treatment. The optimal post-treatment temperature was 300 °C for annealing and 500 °C for both sulfurization and selenization, with a ramp rate of 5 °C/min. The carbon impurities in the precursor film were removed by air annealing, and oxide that was formed during annealing was removed by sulfurization. The fabricated CIGSSe solar cell showed a conversion efficiency of 4.63% for a 0.44 $cm^2$ area, with $V_{oc}$ = 0.4 V, $J_{sc}$ = 21 $mA/cm^2$, and FF = 0.53.

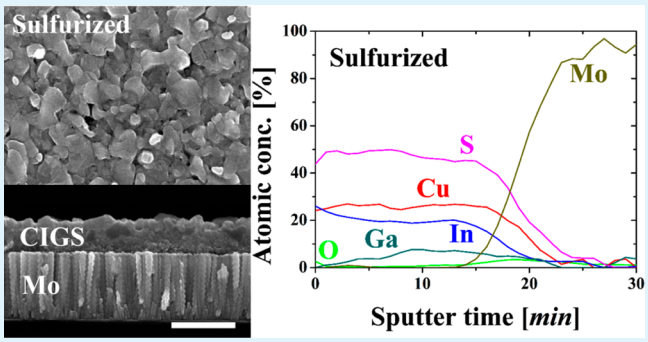


**KEYWORDS:** *CIGSSe, thin film, solar cell, electrostatic spray, carbon free, oxygen free*

## 1. INTRODUCTION

Copper indium gallium selenide (CIGS), a I−III−$VI_2$ semiconductor material with a chalcopyrite crystal structure, is used as an absorber layer for CIGS solar cells, which are considered by many to be the most promising type of thin-film solar cell. The advantages of CIGS include (1) favorable optical and electrical properties, including a direct band gap that is tunable from 1 to 2.4 eV by addition of gallium and sulfur, (2) large photon absorption coefficients, and (3) relatively high power-conversion efficiencies. These advantages have made CIGS a popular material in the thin-film photovoltaic community.[1] In general, the chemical formula of CIGS has the form $CuIn_xGa_{(1-x)}Se_2$, where $x$ can be varied from unity to zero to tune the band gap for optimal performance while maintaining the stoichiometric 1:1:2 compositional ratio.

The highest power-conversion efficiency (PCE or $\eta$) achieved with a CIGS solar cell is approximately $\eta$ = 20%.[2] The absorber film in this case was manufactured by co-evaporation, a vacuum-based method.[2] However, vacuum-based methods (such as co-evaporation and sputtering) have relatively high manufacturing costs because of their high capital and energy requirements.[3] For these reasons, low-cost non-vacuum-based methods (such as printing, pasting, casting, and spraying) provide attractive alternative routes for commercial production of thin-film solar cells. Non-vacuum methods, including spin coating,[4] doctor blading,[5] drop casting,[6] spraying,[7] electrodeposition,[8] ultrasonic spraying,[9] and electrostatic spray deposition,[10] have been used, but they have produced a lower PCE than vacuum-based methods.

The best PCE with non-vacuum methods was obtained by the Mitzi et al.[4] Using a CIGS precursor prepared with hydrazine and applied via spin coating, they achieved a PCE of 15.2%. Hydrazine dissolves binary chalcogenides without the use of any additives that would hinder the solar cell efficiency.

Received: March 3, 2014
Accepted: April 25, 2014
Published: April 25, 2014

   dx.doi.org/10.1021/am501286d | ACS Appl. Mater. Interfaces 2014, 6, 8369−8377

Table 1. Summary of Previously Reported Solution-Processed CIGS Solar Cells

| year | author | precursor type | materials | method | efficiency (%) | FF (%) | $V_{oc}$ (V) | $J_{sc}$ (mA/cm$^2$) |
|---|---|---|---|---|---|---|---|---|
| 2008 | Panthani et al.[14] | particle | CIS, CISe, CIGSe | drop casting | 0.20 | | | |
| 2012 | Yoon et al.[10] | solution | CISe | electrostatic spray | 1.75 | 33.8 | 0.23 | 21.7 |
| 2010 | Ahn et al.[15] | solution | CISe | doctor blade | 1.93 | 28.0 | 0.33 | 20.9 |
| 2012 | Ahn et al.[16] | particle | CISe | doctor blade | 1.98 | 33.0 | 0.27 | 22.6 |
| 2008 | Guo et al.[17] | particle | CIS | drop casting | 2.82 | 39.0 | 0.28 | 25.8 |
| 2012 | Park et al.[18] | solution | CIGSSe | spin coating | 4.32 | 49.0 | 0.45 | 20.1 |
| 2011 | Lee et al.[19] | particle | CIGSe | spin coating | 4.48 | 47.3 | 0.45 | 21.0 |
| **2013** | **present study** | **solution** | **CIGSSe** | **electrostatic spray** | **4.63** | **53.37** | **0.41** | **20.95** |
| 2009 | Guo et al.[6] | particle | CIGSSe | drop casting | 5.50 | 51.5 | 0.46 | 23.7 |
| 2013 | Cai et al.[20] | solution + NP | CISSe | spray | 6.15 | 53.0 | 0.43 | 26.7 |
| 2012 | Ahn et al.[21] | solution | CISe | spin coating | 7.72 | 50.5 | 0.42 | 36.4 |
| 2012 | Wang et al.[22] | solution | CIGSe | spin coating | 8.01 | 59.0 | 0.53 | 25.7 |
| 2012 | Jeong et al.[23] | particle | CISe | casting | 8.20 | 55.0 | 0.44 | 33.7 |
| 2013 | Park et al.[24] | solution | CIGS | spin coating | 8.28 | 61.9 | 0.79 | 17.0 |
| 2012 | Wang et al.[25] | solution | CIGSSe | spin coating | 8.80 | 68.9 | 0.61 | 20.9 |
| 2013 | Guo et al.[5] | particle | CIGSSe | doctor blade | 12.00 | 65.7 | 0.63 | 28.8 |
| 2010 | Liu et al.[26] | solution | CISSe | spin coating | 12.20 | 73.0 | 0.55 | 29.8 |
| 2013 | Todorov et al.[4] | solution | CIGSSe | spin coating | 15.20 | 75.0 | 0.62 | 32.6 |

Despite resulting in a high PCE, it is difficult to envision the widespread use of the hydrazine-based approach because of its toxicity, reactivity, and high cost.[4,11−13] Table 1 briefly summarizes the history of the PCE of CIS-based solar cells.[4−6,10,14−26]

Building upon our previous efforts,[27] we adopted electrostatic spray deposition (ESD) in this study to spray the CIG precursor. The advantages of ESD include the extremely small usage of precursor (nearly 100% deposition efficiency), nanoscale drop generation, and potential for application in large-scale production.[10] Furthermore, we introduce a process for producing carbon- and oxygen-free films via sulfurization and selenization, which improves the overall PCE. After sulfurization and selenization, the electro-sprayed Cu(In,Ga)$(SSe)_2$ (CIGSSe) solar cell had a 4.63% power conversion efficiency with an open-circuit voltage, $V_{OC}$, of 0.41 V, a short-circuit current density, $J_{sc}$, of 20.95 mA/cm$^2$, and a fill factor, FF, of 0.53 on an active absorber area of 0.46 cm$^2$.

## 2. EXPERIMENTAL SECTION

**Precursor Preparation.** Cu−In−Ga (CIG) salts were dissolved in propylene glycol (PG, $C_3H_8O_2$; 99.0%, Duksan Chemical, 10 mL). The use of highly viscous PG resulted in stable jetting from the Taylor cone during electrostatic spraying. The CIG salts used here were copper(II) nitrate hydrate ($Cu(NO_3)_2{\cdot}xH_2O$; 99.999%, Alfa Aesar, 1.0 g), indium(III) nitrate hydrate ($In(NO_3)_3{\cdot}xH_2O$; 99.99%, Alfa Aesar, 1.12 g), and gallium(III) nitrate hydrate ($Ga(NO_3)_3{\cdot}xH_2O$; 99.999%, Alfa Aesar, 0.41 g). All precursor preparations were carried out in air under ambient laboratory conditions. The CIG precursor was dissolved in PG using a magnetic stirrer for 3 h. The standard atomic ratio of each component, Cu/In/Ga, was 1:0.7:0.3. The ratio of Cu/(In + Ga) was kept at unity or slightly under in order to form a chalcopyrite grain structure with a (112) orientation.[28]

**Electrostatic Spray Deposition and Post-Treatment.** The details of the ESD system are described in a previous publication.[10] The voltage applied was in the range of 10−12 kV. The precursor flow rate was about 150 $\mu$L/h. The standoff distance between the nozzle and the molybdenum-coated glass substrate (25 × 25 mm$^2$) was 45 mm with a cone angle of 40°. The typical deposition time for a 1 $\mu$m thick CIG layer was about 20 min. The substrate was heated at 80 °C during spraying, which was followed by 10 min of air annealing at 300 °C, 30 min of sulfurization at 500 °C under a continuous flow of $H_2S$ (1%)/$N_2$ gas (100 sccm), and then 10 min of selenization at 500 °C in the presence of 0.05 g of selenium powder placed near the sample.

**Cell Fabrication.** Solar cells were fabricated with the conventional Mo/CIGSSe/CdS/*i*-ZnO/*n*-ZnO/Ni/Al structure. A 60 nm thick CdS buffer layer was prepared on a CIGSSe absorber by chemical bath deposition, and *i*-ZnO (50 nm)/Al-doped *n*-ZnO (500 nm) TCO layers were deposited by radiofrequency magnetron sputtering. A Ni (50 nm) and Al (500 nm) grid was prepared as a current collector by thermal evaporation. The active area of the completed cell was 0.46 cm$^2$.

**Characterization.** The morphology, composition, and crystalline structure of the precursor films and the selenized films were investigated by high-resolution scanning electron microscopy (HRSEM, XL30SFEG Phillips Co., The Netherlands, 10 kV), energy-dispersive X-ray spectroscopy (EDS, EDAX Genesis Apex, acceleration voltage, 30 kV; collection time, 100 s; with a standardless method), and X-ray diffraction (XRD, Rigaku Japan, D/MAX-2500, with Cu K$\alpha$ radiation). The compositional profile and depth of the selenized film were determined by Auger electron spectroscopy (AES, PerkinElmer, SAM4300). Device performance measures including the conversion efficiency and the external quantum efficiency (EQE) were measured with a class AAA solar simulator (WXS-155S-L2, WACOM, Japan) under the AM1.5 conditions.

## 3. RESULTS AND DISCUSSION

The PCE of a cell based on a similarly electrosprayed $CuInSe_2$ (CIS) film was 1.75% in previous work.[10] The low efficiency was due to a relatively thick (~600 nm) amorphous carbon layer that originated from the binder materials of the CIS precursor. During crystallization of the film via selenization, the binder material evaporated as the top surface of the CIS film crystallized. This crystallized surface on top prevented further evaporation of the binder. As a result, the carbon layer remained in the film and acted as a substantial resistor, which caused a low fill factor and cell efficiency. Furthermore, the carbon impurity layer often produced delamination of the CIGS absorber layer because of its poor adhesion to the molybdenum substrate. Other studies have reported that the carbon layer constrains CIGS crystal growth.[15,29] For these reasons, it is the best to remove the carbon layer to improve the overall conversion efficiency. Park et al.[18,19] introduced air annealing immediately after coating a CIGS absorber layer to remove carbon from the CIGS layer. They noted that an

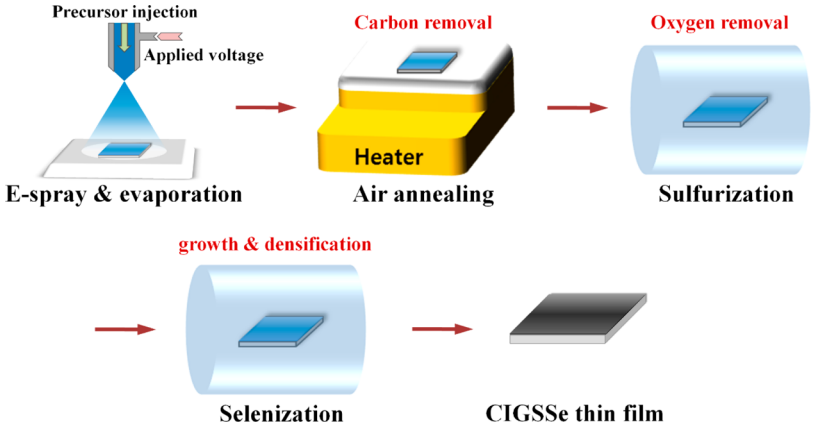


**Figure 1.** Schematic of the CIGSSe thin-film fabrication processes.

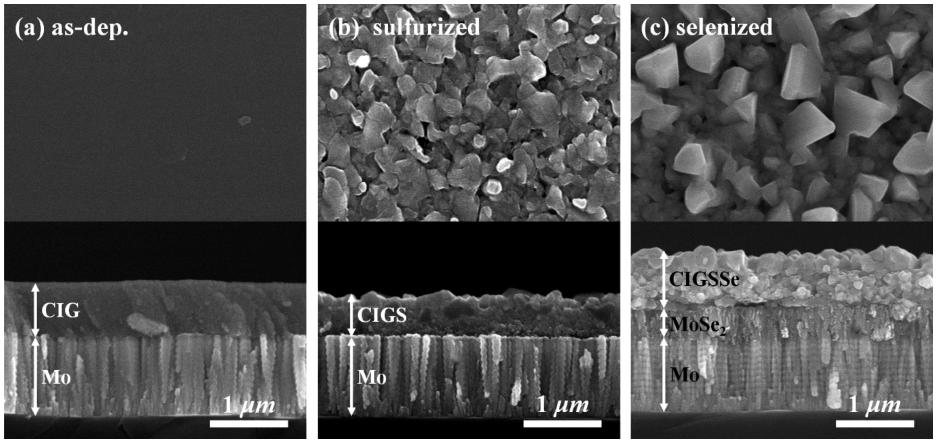


**Figure 2.** Top-view (top row) and cross-sectional (bottom row) SEM images of the (a) as-deposited CuInGa film, (b) sulfurized $Cu(InGa)S_2$ film, and (c) selenized $Cu(InGa)(SSe)_2$ film.

annealing temperature of 350 °C was optimal; higher temperatures resulted in oxidation of the molybdenum substrate, which reduced the solar cell efficiency.

We adopted an air-annealing process to remove carbon impurities from the Cu−In−Ga precursor film. Then, oxide that was formed during annealing was removed via sulfurization. Selenization followed as a final step to grow the CIGS grains. These procedures are illustrated in Figure 1. Figure 2a shows the as-deposited nanocrystalline CuInGa precursor film with a film thickness of ∼0.8 μm. The air-annealed metallic precursor film was sulfurized in a $H_2S$ atmosphere to remove residual oxide, forming a very dense and crack-free flat surface morphology. The thickness of the sulfurized CIGS absorber was reduced to ∼0.5 μm, as shown in Figure 2b. After selenization, larger grains are formed, as shown in Figure 2c. A molybdenum diselenide ($MoSe_2$) layer with a thickness of 0.2 μm was formed at the interface between the CIGS absorber and the molybdenum substrate.

**Effects of Annealing.** CuInGa precursor with an atomic ratio of 1:0.7:0.3 was electrosprayed onto the molybdenum-coated soda-lime glass for 20 min. The substrate was heated at 80 °C to dry the film followed by 10 min of annealing at higher temperature (200 °C or higher) in air. Annealing was necessary to remove carbon residues or impurities, even though it produced oxides. Figure 3 shows the effect of the annealing temperature on the surface morphology of the CIG precursor film. No difference was observed between the films annealed at

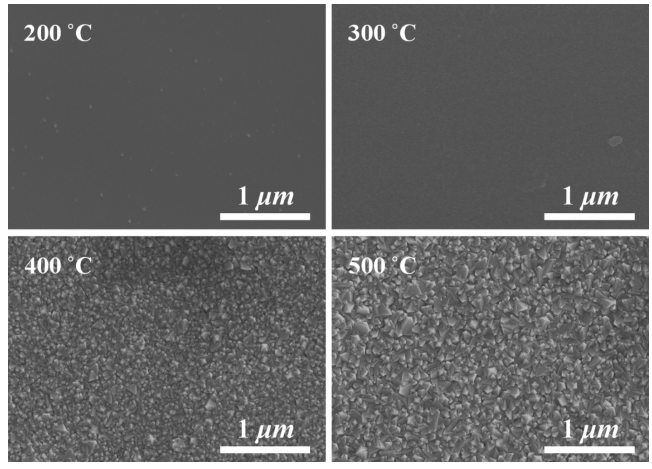


**Figure 3.** Top-view SEM images showing the effect of the air-annealing temperature on the surface morphology and grain size of the as-deposited film (before sulfurization).

200 °C and those annealed at 300 °C. At annealing temperatures of 400 °C or higher, growth of crystal grains was clearly visible. Figure 4 shows the powder XRD patterns for the films shown in Figure 3. No clear peaks are seen following annealing at 200 or 300 °C, even though oxides were formed during annealing. In Figure 3, peaks corresponding to $In_2O_3$ are observed after annealing at 400 and 500 °C, which is


dx.doi.org/10.1021/am501286d | ACS Appl. Mater. Interfaces 2014, 6, 8369−8377

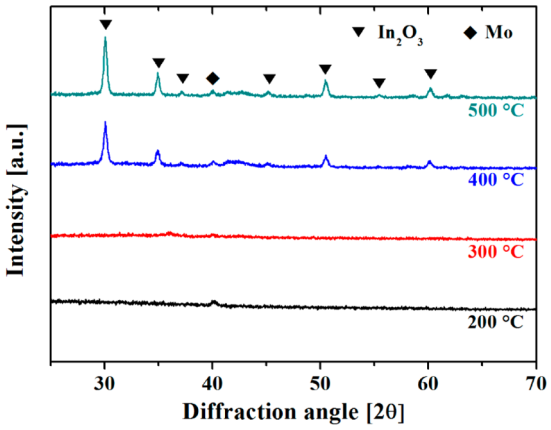


**Figure 4.** XRD of air-annealed Cu−In−Ga films.

undesirable because its presence greatly hinders the electrical mobility of the cell.

**Sulfurization.** Sulfurization was performed after the annealing procedure to remove the oxides formed during annealing. Sulfurization of the CIGO film was carried out under $H_2S(1\%)/N_2$ gas for 30 min at various temperatures. The sulfurization procedure resulted in the formation of $CuInGaS_2$, which on its own can function as a solar cell device. However, we introduced the additional selenization post-treatment to grow CIGS grains and to replace sulfur with selenium.

We have observed the effect of sulfurization at 500 °C, which is shown in Figure 2b. Figure 5 shows a comparison of the

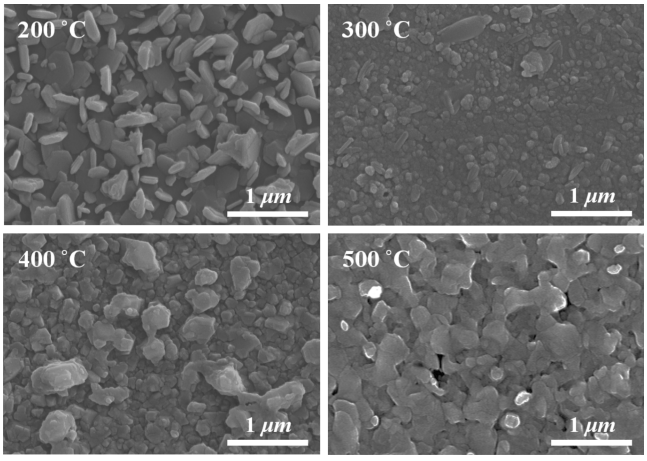


**Figure 5.** Top-view SEM images showing the effect of sulfurization temperature on surface morphology and grain size.

surface morphology of the CIGS films produced at various sulfurization temperatures. At 300 °C and above, higher temperatures resulted in larger grain sizes. The corresponding XRD results shown in Figure 6a provide information on the crystallinity and phase of the sulfurized films shown in Figure 5. As the sulfurization temperature increased from 300 to 500 °C, the peak intensity also increased and the peak width decreased, which is consistent with the surface morphology observed in the SEM images in Figure 5. At 200 °C, the film was in an amorphous state. However, above 300 °C, the films were well-crystallized to form $Cu(InGa)S_2$.

Figure 6b shows the diffraction patterns, crystallite size, and lattice parameter of the $Cu(InGa)S_2$ film sulfurized at 500 °C. The solid line is the typical XRD pattern of a $CuInS_2$ crystalline structure, which is compared to the crystalline structure of our $Cu(InGa)S_2$ film. The lack of a discernable difference in the XRD patterns suggests that the gallium content in the $Cu(InGa)S_2$ film was low. The values for the lattice parameters are also much closer to those of $CuInS_2$ than to those of $CuInSe_2$. In addition, comparison with JCPDS card no. 85-1575 confirmed that the crystal structure of our $Cu(InGa)S_2$ film is body-centered tetragonal, with unit cell parameters of $a = b = 5.522$ and $c = 11.132$.

Figure 7 shows the atomic concentration of each component included in the film, as determined using Auger electron spectroscopy (AES). The $x$ axis indicates the sputter time elapsed during the AES characterization, which implies the depth of the film. The sharp rise of the molybdenum content implies the interface between the deposited absorber layer and the molybdenum substrate. In Figure 7a, the oxide content is prevalent as a result of air annealing in the previous post-treatment step. The atomic ratio of Cu/(In + Ga) was maintained at unity (i.e., $30/(20 + 10) \sim 1$) before sulfurization. This ratio is nearly the same as the atomic concentration of the initial precursor: In/Cu ∼ 0.67 and Ga/Cu ∼ 0.33. Therefore, air annealing alone did not alter the initial atomic concentration of the precursor even though annealing caused oxide formation throughout the entire film. Figure 7b shows the compositional changes of each element after sulfurization. As expected, most oxides were removed as their atomic concentrations neared zero for the range of sputter times from 0−15 min. The oxygen content observed at sputter times greater than 15 min is indicative of the formation of molybdenum oxide, which was removed later during selenization. The sulfur content was dominant after sulfurization. The ideal composition of the elements is 1:1:2 for Cu/(In + Ga)/S, which seems to be the case, as shown in Figure 7b. It is noteworthy that some Ga was lost during the sulfurization process. The copper content was slightly reduced, which is also desirable because a copper-poor condition is essential to form a chalcopyrite grain structure with (112) orientation.[28] CuInGaS alone without selenium can function as a solar cell device. However, we introduced an additional selenization process step to grow the grains of the CIGS film and to tune the band gap of the absorber layer

**Selenization.** The sulfurized films were selenized to grow the CIGSSe absorber layer at various temperatures of 300, 400, 500, 520, 540, and 560 °C. The ramp rate was 5 °C/min for each temperature. The selenization process lasted for 10 min under nitrogen gas. Figure 8 shows the XRD results for the $Cu(InGa)(SSe)_2$ (CIGSS) films selenized at various temperatures. At 300 and 400 °C, the sulfurized film was not selenized, as the low-selenization-temperature results did not have an apparent peak for CIGSS; only the three peaks corresponding to CIGS (CuInGaS) are apparent. At 500 °C, the CIGSS peaks are clearly shown. In fact, the peaks at 500 °C are the sharpest when compared to the peaks at higher temperatures. Table 2 summarizes the crystal size of the films selenized at various temperatures. The crystal size was estimated using the Debye−Scherrer formula,[30] $D = k\lambda/(\beta \cos \theta)$, where $D$ is the mean grain size, $k$ is a geometric factor (0.89), $\lambda$ is the X-ray wavelength, $\beta$ is the full width at half-maximum (fwhm) of the diffraction peak, and $\theta$ is the diffraction angle. The results confirmed that the largest crystal size was found at the selenization temperature of 500 °C.

In addition to the selenization temperature, the temperature ramp rate (or selenization duration) has a substantial influence

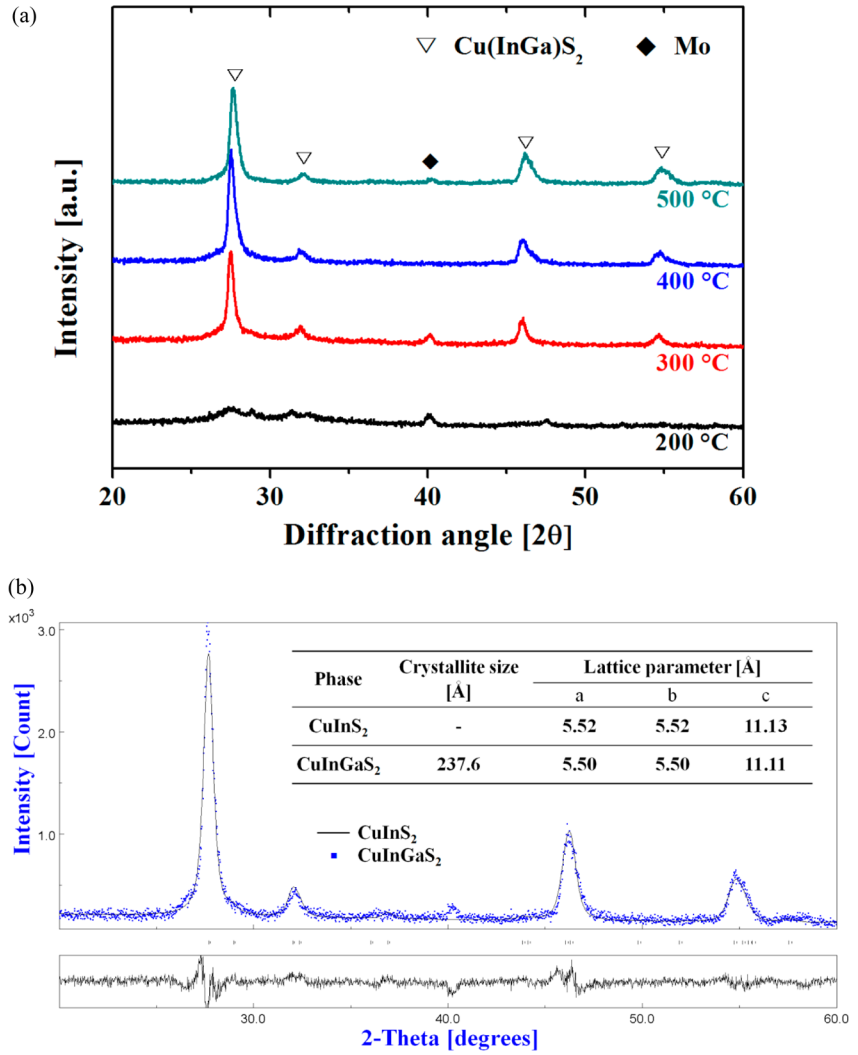


**Figure 6.** (a) XRD of films after sulfurization. (b) XRD patterns with Rietveld refinement fits to the film sulfurized at 500 °C.

on the surface morphology and the crystallization of the films. Figure 9 shows the surface morphology of the films selenized at 500 °C with various temperature ramp rates. The largest crystal size is found in the case with 100 min. This qualitative observation is confirmed by the XRD results shown in Figure 10. Although the differences are subtle, the peak is the sharpest (lowest fwhm) in the case with the ramp time of 100 min. The crystal sizes of these films selenized at various increase rates are summarized in Table 3, which also quantitatively confirms that increasing the temperature over 100 min produced the largest grain size during the selenization process. Table 4 summarizes the optimal post-treatment conditions, starting from air annealing to sulfurization and selenization.

**Cell Fabrication.** The electrosprayed CIGSS absorber layer was about 0.7 $\mu$m thick, whereas it is well-known that an absorber layer of 1 to 2 $\mu$m is optimal to increase light absorption, thereby increasing electrical current as well.[29] Thinner layers introduce increased recombination with the back contact, which in turn decreases carrier collection and eventually reduces the PCE.[31] We also fabricated an absorber layer thicker than 1 $\mu$m. As for the thinner film, air annealing produced a carbon-free dense film. However, when the thickness of this dense film was greater than 1 $\mu$m, then selenizing this dense film became very difficult because selenium cannot readily infiltrate into the absorber film. In the case of a thicker layer, only the top surface was selenized. The selenized top layer then functioned as a blocking layer that prevented further penetration of selenium into the remainder of the film. For these reasons, we produced devices with an absorber layer that was less than 1 $\mu$m thick, which allowed complete permeation of selenium into the entire film, leading to successful selenization.

Permeation of the selenium vapor into the deep bottom part of the absorber layer is not always desirable because the permeated gas reacts with molybdenum and forms $MoSe_2$, as indicated in Figure 2c. This formation of a $MoSe_2$ layer at the interface between the absorber layer and the Mo substrate has often been reported, especially when the selenium gas pressure is relatively high. Thus, the correct selenium gas pressure is crucial to provide sufficiently high penetration of the gas into the film while still being low enough to minimize the formation of the $MoSe_2$ layer.[23]

A CIGSS solar cell was fabricated with the conventional Mo/CIGSSe/CdS/*i*-ZnO/*n*-ZnO/Ni/Al structure on an active cell area of 0.46 $cm^2$, with a depth profile having various elements, as shown in Figure 11. The content of Cu, In, Ga, and S in the absorber layer is lower toward the back contact, whereas the Se content is greater at the interface between the absorber layer

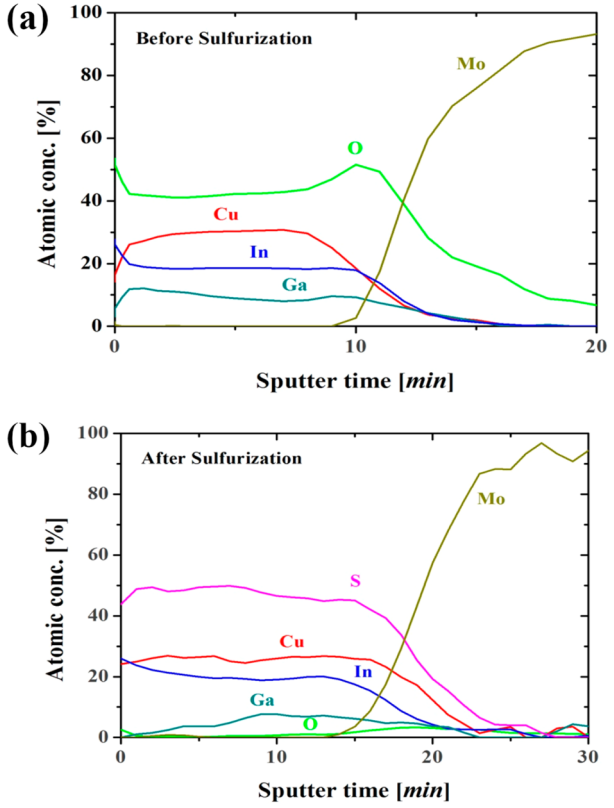


**Figure 7.** Effect of sulfurization. The AES depth profiles shows the atomic concentration of each element for the film (a) prior to sulfurization and (b) after sulfurization.

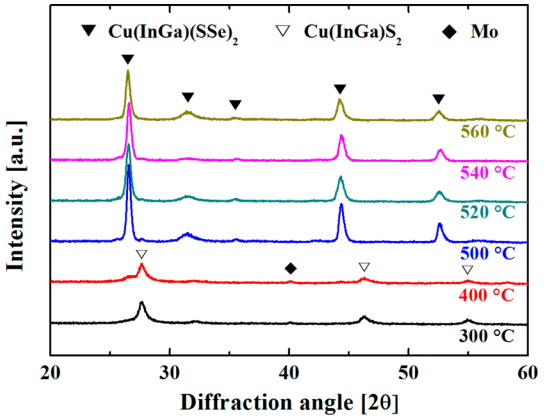


**Figure 8.** Effect of selenization temperature on CIGSS crystallization.

**Table 2. Crystal Size Variation with Selenization Temperature**

| selenization temperature (°C) | 300 | 400 | 500 | 520 | 540 | 560 |
|---|---|---|---|---|---|---|
| crystal size (nm) | 26.9 | 24.3 | 42.3 | 36.8 | 40 | 37.8 |

and the substrate, which is evidence for the formation of $MoSe_2$. The presence of S and Se confirms that this solar cell is of the $CuInGa(SSe)_2$ type. The zinc and oxygen contents in the range of 15−30 min represent the ZnO window layer stacked during cell/device fabrication. The absorber layer is essentially carbon- and oxygen-free, as there is no carbon or oxygen content. It is well-known that a slightly copper-poor condition, such as $0.86 < Cu/(In + Ga) < 0.96$,[32,33] yields the best solar cell performance. A sputter time between 30 and 45 min was approximated for the absorber layer to meet copper-poor conditions (i.e., $Cu/(In + Ga) < 1$). The ratio between (Se + S) and (Cu + In + Ga + S + Se) was also kept near 0.5. Retaining the optimal compositions is challenging because the composition ratio changes during the multiple post-treatments.[15,23,34]

Figure 12 shows a comparison of the XRD patterns of the annealed CuInGa, sulfurized $CuInGaS_2$, and selenized $CuInGa(SSe)_2$ absorber. It can be seen that the as-deposited precursor film is amorphous in nature. After sulfurization, the films are polycrystalline and exhibit four characteristic CIGS peaks along the (112), (200), (204)/(204), and (312) directions at $2\theta$ values of 28.20, 32.58, 47.32, and 56.17, respectively (CIS, JCPDS card no. 85-1575). After selenization, the entire XRD pattern shifts toward lower angle with higher peak intensities and narrower peak widths, indicating the CIGSSe polycrystalline state (JCPDS card no. 36-1311). The shift toward the lower angles (which are 27.25° (112), 45.3° (220/204), and 53.7° (116/312)) was due to unit cell volume expansion when replacing sulfur with selenium.[25] Comparing the CIGS peaks with the CIGSSe peaks, the CIGSSe peaks are sharper and larger, which is indicative of larger grain size. Thus, selenization certainly helped to increase the grain size, which can also be observed visually in Figure 2b,c.

Figure 13a shows the EQE measurement of the CIGSSe solar cell for a wavelength range from 300 to 1200 nm. The short-wavelength region is strongly influenced by absorption by the TCO (ZnO) and CdS-buffer layers. The EQE spectrum exhibits a sharp maximum around 550 nm at a level of 0.61, which is lower than values reported in the literature.[2] On the basis of the EQE measurement, the energy loss of the short-circuit current was dominated by poor carrier collection efficiency in the range between 650 and 1100 nm. Back contact recombination, short minority carrier lifetime, and insufficient thickness of the absorber layer all contribute to the suboptimal performance of the solar cell. Defects residing in the back contact area caused the short carrier lifetime and the recombination effects. Smaller grain sizes correspond to a higher density of grain boundaries. This increases recombination of electron−hole pairs at grain boundaries, which in turn reduces solar cell efficiency. Figure 2c shows well-crystallized larger grains in the upper part of the absorber layer, whereas relatively smaller grains are found in the lower part. The smaller grains in the lower part of the absorber layer increase recombination and reduce the carrier lifetime. It is also known that the quantum efficiency (QE) is reduced if the absorber layer is less than 1 $\mu$m thick, as compared to the QE of a film with 1 to 2 $\mu$m thickness.[31] The effect of a thin absorber layer is most evident at longer wavelengths, where the absorbance of the film is lower. Thus, a large grain size, which minimizes voids and grain boundaries, and sufficiently thick absorber layer are required to maximize the QE.

Figure 13b shows the estimated band gap of the absorber layer based on the EQE data. The estimation was made by plotting $[h\nu \times \ln(1 - EQE)]^2$ versus $h\nu$ and drawing a tangent line. The tangent line intersects the $x$ axis at the band gap energy of the absorber layer, which is about 1.15 eV. This estimation is similar to the values reported in the literature.[4,25,35,36]

As indicated in Figure 11, the atomic concentration ratio of $Cu/(In + Ga)$ is not consistent over the depth of the absorber layer. We also noted that the thickness of the absorber layer was


dx.doi.org/10.1021/am501286d | ACS Appl. Mater. Interfaces 2014, 6, 8369−8377

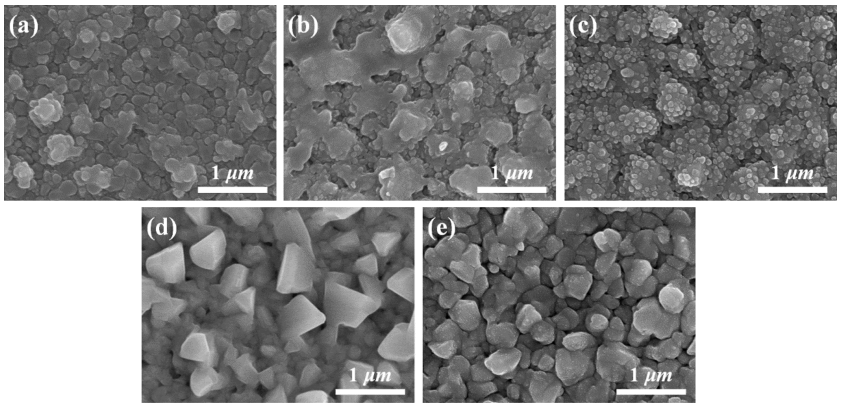


**Figure 9.** Top-view SEM images showing the surface morphology of the films after selenization. The influence of the time over which the sample was heated to the selenization temperature (temperature ramp time) on the surface morphology, for temperature ramp times of (a) 10, (b) 30, (c) 60, (d) 100, and (e) 130 min.

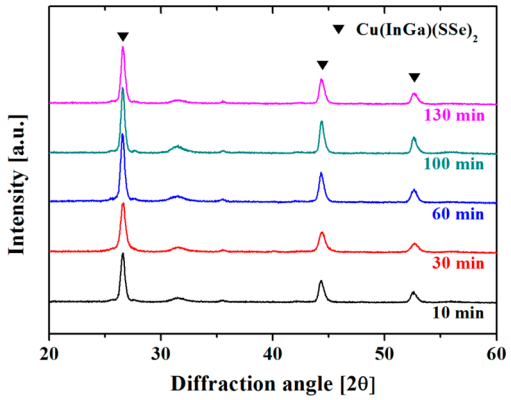


**Figure 10.** XRD after selenization with varying heating rates to give temperature ramp times of 10, 30, 60, 100, and 130 min at a selenization temperature of 500 °C.

**Table 3. Crystal Size Variation with Selenization Temperature Ramp Time**

| time (min) | 10 | 30 | 60 | 100 | 130 |
|---|---|---|---|---|---|
| crystal size (nm) | 33.4 | 38.5 | 38.6 | 42.3 | 39.5 |

**Table 4. Optimized Post-Treatment Conditions**

| | |
|---|---|
| air-annealing temp. (°C) | 300 |
| sulfurization temp. (°C) | 500 |
| selenization temp. (°C) | 500 |
| selenization time (min) | 100 |

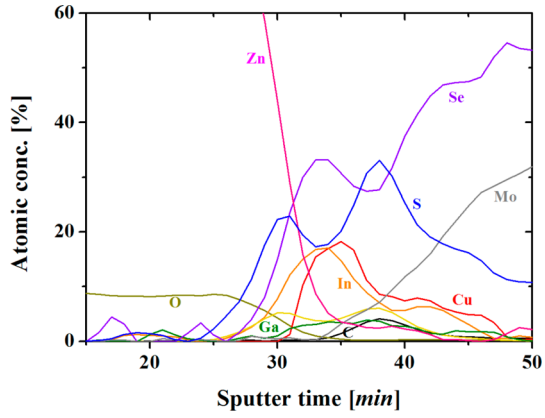


**Figure 11.** AES depth profile of the cell fabricated under the optimal conditions: annealing temperature of 300 °C, sulfurization temperature of 500 °C, selenization temperature of 500 °C, and a selenization ramp time of 100 min.

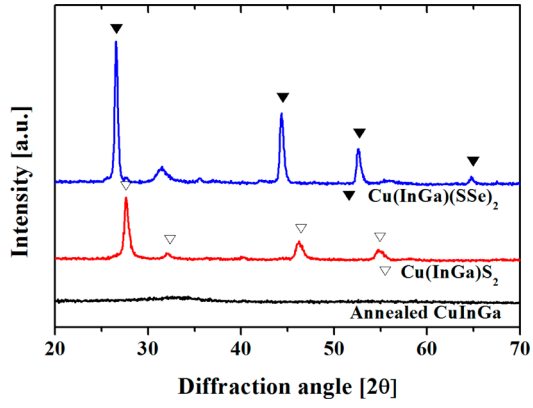


**Figure 12.** XRD pattern of the film annealed at 300 °C, sulfurized at 500 °C, and selenized at 500 °C with ramp time of 100 min.

not sufficiently high (less than 1 μm), which hinders the absorbance of photons of longer wavelength. Furthermore, the formation of $MoSe_2$ at the interface between the absorber layer and the molybdenum substrate is excessive. Figure 14 shows the $I-V$ characteristics of our electrosprayed CIGSSe thin-film solar cell device. The best solar cell processed so far achieved a PCE of 4.63% with an open-circuit voltage ($V_{oc}$) of 0.41 V, a short-circuit density ($J_{sc}$) of 21 mA/cm$^2$, and a fill factor (FF) of 0.53 for an active area of 0.46 cm$^2$. This PCE value represents a 2.5-fold increase from our previous record.[10] The carbon- and oxygen-free approaches introduced in this study clearly helped to improve the PCE value. In addition, the band gap value increased from 1.02 eV in our previous work to 1.15 eV here because of the inclusion of gallium. The widened band gap is closer to the theoretically optimal value of 1.34 eV for a single-junction cell and therefore provides an improved PCE.

## 4. CONCLUSIONS

We demonstrated the synthesis of carbon- and oxygen-free $Cu(InGa)(SSe)_2$ (CIGSSe) absorber thin films prepared by electrospraying a CuInGa precursor followed by sulfurization and selenization at elevated temperature. A polycrystalline


dx.doi.org/10.1021/am501286d | ACS Appl. Mater. Interfaces 2014, 6, 8369−8377

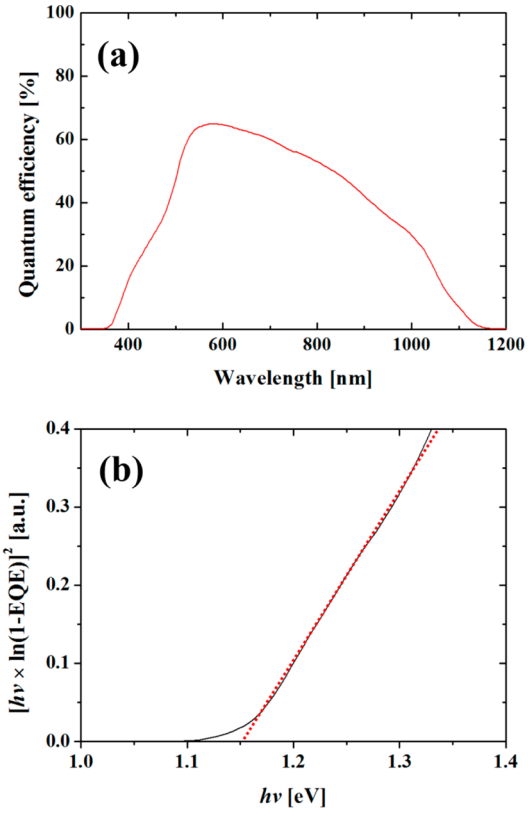


**Figure 13.** (a) External quantum efficiency and (b) estimation of the band gap.

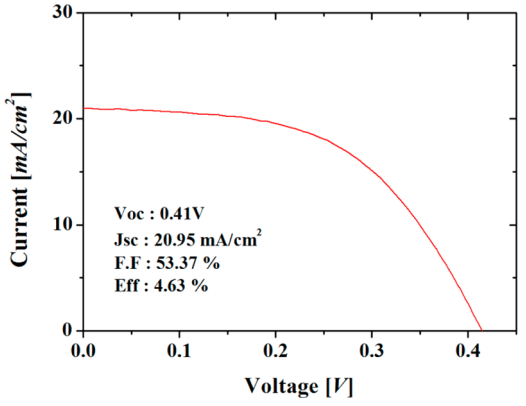


**Figure 14.** *I*–*V* characteristics of the CIGSSe solar cell on a molybdenum-coated substrate.

chalcopyrite CIGSSe absorber with a large-faceted flat-grained morphology was prepared after sulfurization and selenization. A solar cell with a 4.63% conversion efficiency was produced with $V_{oc}$ = 410 mV, $J_{sc}$ =21 mA/cm$^2$, and FF = 0.5337 for an active area of 0.46 cm$^2$.

## AUTHOR INFORMATION

### Corresponding Author

*E-mail: skyoon@korea.ac.kr.

### Author Contributions

◆H.Y. and S.H.N. contributed equally to this work.

### Notes

The authors declare no competing financial interest.

## ACKNOWLEDGMENTS

This work was supported by the Human Resources Development Program (no. 20124030200120) of KETEP and also by the Industrial Strategic Technology Development Program (10045221) of MKE. The authors extend their appreciation to the Deanship of Scientific Research at King Saud University for funding the work through the research group project no. RGP-089.

## REFERENCES

(1) Romeo, A.; Terheggen, M.; Abou-Ras, D.; Bätzner, D. L.; Haug, F. J.; Kälin, M.; Rudmann, D.; Tiwari, A. N. Development of Thin-Film Cu(In,Ga)Se$_2$ and CdTe Solar Cells. *Prog. Photovoltaics* **2004**, *12*, 93–111.

(2) Jackson, P.; Hariskos, D.; Lotter, E.; Paetel, S.; Wuerz, R.; Menner, R.; Wischmann, W.; Powalla, M. New World Record Efficiency for Cu(In,Ga)Se$_2$ Thin-Film Solar Cells Beyond 20%. *Prog. Photovoltaics* **2011**, *19*, 894–897.

(3) Eberspacher, C.; Fredric, C.; Pauls, J.; Serra, K. Thin-Film CIS Alloy PV Materials Fabricated Using Non-Vacuum, Particles-Based Techniques. *Thin Solid Films* **2001**, *387*, 18–22.

(4) Todorov, T. K.; Gunawan, O.; Gokmen, T.; Mitzi, D. B. Solution-Processed Cu(In,Ga)(S,Se)$_2$ Absorber Yielding a 15.2% Efficient Solar Cell. *Prog. Photovoltaics* **2013**, *21*, 82–87.

(5) Guo, Q.; Ford, G. M.; Agrawal, R.; Hillhouse, H. W. Ink Formulation and Low-Temperature Incorporation of Sodium to Yield 12% Efficient Cu(In,Ga)(S,Se)$_2$ Solar Cells from Sulfide Nanocrystal Inks. *Prog. Photovoltaics* **2013**, *21*, 64–71.

(6) Guo, Q.; Ford, G. M.; Hillhouse, H. W.; Agrawal, R. Sulfide Nanocrystal Inks for Dense Cu(In$_{1-x}$Ga$_x$)(S$_{1-y}$Se$_y$)$_2$ Absorber Films and Their Photovoltaic Performance. *Nano Lett.* **2009**, *9*, 3060–3065.

(7) Ahn, S.; Kim, K. H.; Yun, J. H.; Yoon, K. H. Effects of Selenization Conditions on Densification of Cu(In,Ga)Se$_2$ (CIGS) Thin Films Prepared by Spray Deposition of CIGS Nanoparticles. *J. Appl. Phys.* **2009**, *105*, 113533–113537.

(8) Duchatelet, A.; Sidali, T.; Loones, N.; Savidand, G.; Chassaing, E.; Lincot, D. 12.4% Efficient Cu(In,Ga)Se$_2$ Solar Cell Pprepared from One Step Electrodeposited Cu–In–Ga Oxide Precursor Layer. *Sol. Energy Mater. Sol. Cells* **2013**, 241–245.

(9) Lee, D.-Y.; Kim, J. Deposition of CuInS$_2$ Films by Electrostatic Field Assisted Ultrasonic Spray Pyrolysis. *Sol. Energy Mater. Sol. Cells* **2011**, *95*, 245–249.

(10) Yoon, H.; Woo, J. H.; Joshi, B.; Ra, Y. M.; Yoon, S. S.; Kim, H. Y.; Ahn, S. J.; Yun, J. H.; Gwak, J.; Yoon, K. H.; James, S. C. CuInSe$_2$ (CIS) Thin Film Solar Cells by Electrostatic Spray Deposition. *J. Electrochem. Soc.* **2012**, *159*, H444–H449.

(11) Mitzi, D.; Yuan, M.; Liu, W.; Kellock, A.; Chey, S.; Deline, V.; Schrott, A. A High-Efficiency Solution-Deposited Thin-Film Photovoltaic Device. *Adv. Mater.* **2008**, *20*, 3657–3662.

(12) Mitzi, D. Solution Processing of Chalcogenide Semiconductors via Dimensional Reduction. *Adv. Mater.* **2009**, *21*, 3141–3158.

(13) Mitzi, D. B.; Todorov, T. K.; Gunawan, O.; Yuan, M.; Cao, Q.; Liu, W.; Reuter, K. B.; Kuwahara, M.; Misumi, K.; Kellock, A. J. Towards Marketable Efficiency Solution-Processed Kesterite and Chalcopyrite Photovoltaic Devices. *IEEE Photovoltaic Spec. Conf., 35th* **2010**, 000640–000645.

(14) Panthani, M. G.; Akhavan, V.; Goodfellow, B.; Schmidtke, J. P.; Dunn, L.; Dodabalapur, A.; Barbara, P. F.; Korgel, B. A. Synthesis of CuInS$_2$, CuInSe$_2$, and Cu(In$_x$Ga$_{1-x}$)Se$_2$ (CIGS) Nanocrystal "Inks" for Printable Photovoltaics. *J. Am. Chem. Soc.* **2008**, *130*, 16770–16777.

(15) Ahn, S.; Kim, C.; Yun, J. H.; Gwak, J.; Jeong, S.; Ryu, B.-H.; Yoon, K. CuInSe$_2$ (CIS) Thin Film Solar Cells by Direct Coating and Selenization of Solution Precursors. *J. Phys. Chem. C* **2010**, *114*, 8108–8113.

(16) Ahn, S.; Kim, K.; Cho, A.; Gwak, J.; Yun, J. H.; Shin, K.; Yoon, K. CuInSe$_2$ (CIS) Thin Films Prepared from Amorphous Cu–In–Se Nanoparticle Precursors for Solar Cell Application. *ACS Appl. Mater. Interfaces* **2012**, *4*, 1530–1536.

(17) Guo, Q.; Kim, S. J.; Kar, M.; Shafarman, W. N.; Birkmire, R. W.; Stach, E. A.; Agrawal, R.; Hillhouse, H. W. Development of $CuInSe_2$ Nanocrystal and Nanoring Inks for Low-Cost Solar Cells. *Nano Lett.* **2008**, *8*, 2982−2987.
(18) Park, S. J.; Lee, E.; Jeon, H. S.; Gwak, J.; Oh, M.-K.; Min, B. K. Oxidation Effects on $CuIn_xGa_{1-x}Se_yS_{2-y}$ Thin Film Growth by Solution Processes. *Thin Solid Films* **2012**, *520*, 3048−3053.
(19) Lee, E.; Park, S. J.; Cho, J. W.; Gwak, J.; Oh, M.-K.; Min, B. K. Nearly Carbon-Free Printable CIGS Thin Films for Solar Cell Applications. *Sol. Energy Mater. Sol. Cells* **2011**, *95*, 2928−2932.
(20) Cai, Y.; Ho, J. C.; Batabyal, S. K.; Liu, W.; Sun, Y.; Mhaisalkar, S. G.; Wong, L. H. Nanoparticle-Induced Grain Growth of Carbon-Free Solution-Processed $CuIn(S,Se)_2$ Solar Cell with 6% Efficiency. *ACS Appl. Mater. Interfaces* **2013**, *5*, 1533−1537.
(21) Ahn, S.; Son, T. H.; Cho, A.; Gwak, J.; Yun, J. H.; Shin, K.; Ahn, S. K.; Park, S. H.; Yoon, K. $CuInSe_2$ Thin-Film Solar Cells with 7.72% Efficiency Prepared via Direct Coating of a Metal Salts/Alcohol-Based Precursor Solution. *ChemSusChem* **2012**, *5*, 1773−1777.
(22) Wang, W.; Han, S. Y.; Sung, S. J.; Kim, D. H.; Chang, C. H. 8.01% $CuInGaSe_2$ Solar Cells Fabricated by Air-Stable Low-Cost Inks. *Phys. Chem. Chem. Phys.* **2012**, *14*, 11154−11159.
(23) Jeong, S.; Lee, B.-S.; Ahn, S.; Yoon, K.; Seo, Y.-H.; Choi, Y.; Ryu, B.-H. An 8.2% Efficient Solution-Processed $CuInSe_2$ Solar Cell Based on Multiphase $CuInSe_2$ Nanoparticles. *Energy Environ. Sci.* **2012**, *5*, 7539−7542.
(24) Park, S. J.; Cho, J. W.; Lee, J. K.; Shin, K.; Kim, J.-H.; Min, B. K. Solution Processed High Band-Gap $CuInGaS_2$ Thin Film for Solar Cell Applications. *Prog. Photovoltaics* **2014**, *22*, 122−128.
(25) Wang, G.; Wang, S.; Cui, Y.; Pan, D. A Novel and Versatile Strategy to Prepare Metal−Organic Molecular Precursor Solutions and Its Application in $Cu(In,Ga)(S,Se)_2$ Solar Cells. *Chem. Mater.* **2012**, *24*, 3993−3997.
(26) Liu, W.; Mitzi, D. B.; Yuan, M.; Kellock, A. J.; Chey, S. J.; Gunawan, O. 12% Efficiency $CuIn(Se,S)_2$ Photovoltaic Device Prepared Using a Hydrazine Solution Process. *Chem. Mater.* **2010**, *22*, 1010−1014.
(27) Yoon, H.; Woo, J. H.; Ra, Y. M.; Yoon, S. S.; Kim, H. Y.; Ahn, S.; Yun, J. H.; Gwak, J.; Yoon, K.; James, S. C. Electrostatic Spray Deposition of Copper−Indium Thin Films. *Aerosol Sci. Technol.* **2011**, *45*, 1448−1455.
(28) Bougnot, J.; Duchemin, S.; Savelli, M. Chemical Spray Pyrolysis of $CuInSe_2$ Thin Films. *Sol. Cells* **1986**, *16*, 221−236.
(29) Kaelin, M.; Rudmann, D.; Kurdesau, F.; Zogg, H.; Meyer, T.; Tiwari, A. N. Low-Cost CIGS Solar Cells by Paste Coating and Selenization. *Thin Solid Films* **2005**, *480-481*, 486−490.
(30) John, R.; Florence, S. S. Structural and Optical Properties of ZnS Nanoparticles Synthesized by Solid State Reaction Method. *Chalcogenide Lett.* **2009**, *6*, 535−539.
(31) Lundberg, O.; Bodegård, M.; Malmström, J.; Stolt, L. Influence of the $Cu(In,Ga)Se_2$ Thickness and Ga Grading on Solar Cell Performance. *Prog. Photovoltaics* **2003**, *11*, 77−88.
(32) Contreras, M. A.; Tuttle, J.; Gabor, A.; Tennant, A.; Ramanathan, K.; Asher, S.; Franz, A.; Keane, J.; Wang, L.; Scofield, J.; Noufi, R. High Efficiency $Cu(In,Ga)Se_2$-Based Solar Cells: Processing of Novel Absorber Structures. *Conf. Rec. IEEE Photovoltaic Spec. Conf., 24th* **1994**, 68−75.
(33) Kemell, M.; Ritala, M.; Leskelä, M. Thin Film Deposition Methods for $CuInSe_2$ Solar Cells. *Crit. Rev. Solid State Mater. Sci.* **2005**, *30*, 1−31.
(34) Park, M.; Ahn, S.; Yun, J. H.; Gwak, J.; Cho, A.; Ahn, S.; Shin, K.; Nam, D.; Cheong, H.; Yoon, K. Characteristics of $Cu(In,Ga)Se_2$ (CIGS) Thin Films Deposited by a Direct Solution Coating Process. *J. Alloys Compd.* **2012**, *513*, 68−74.
(35) Mitzi, D. B.; Yuan, M.; Liu, W.; Kellock, A. J.; Chey, S. J.; Gignac, L.; Schrott, A. G. Hydrazine-Based Deposition Route for Device-Quality CIGS Films. *Thin Solid Films* **2009**, *517*, 2158−2162.
(36) Yuan, M.; Mitzi, D. B.; Liu, W.; Kellock, A. J.; Chey, S. J.; Deline, V. R. Optimization of CIGS-Based PV Device through Antimony Doping. *Chem. Mater.* **2009**, *22*, 285−287.